Geophysical Journal International

Geophys. J. Int. (2010) **181,** 1247–1260 doi: 10.1111/j.1365-246X.2010.04578.x

Crustal structure of the Tethyan Himalaya, southern Tibet: new constraints from old wide-angle seismic data

Zhongjie Zhang[1] and Simon Klemperer[2]

[1]*State Key Laboratory of Lithospheric Evolution, Institute of Geology and Geophysics, Chinese Academy of Sciences, Beijing* 100029*, China. E-mail: zhangzj@mail.iggcas.ac.cn*

[2]*Department of Geophysics, Stanford University, Stanford,* CA 94305-2215*, USA*

Accepted 2010 February 23. Received 2010 February 11; in original form 2009 September 21

SUMMARY

A wide-angle seismic profile between Peigu Tso (85.5°E) and Pumoyong Tso (90.5°E) in southern Tibet, acquired under a joint Sino-French program in 1981, passes through the South Tibetan Detachment System (STDS, the eastern segment of the profile) and the central part of the Tethyan Himalaya (the western segment). We herein reinterpret this wide-angle seismic profile, which has a total length of ∼480 km, in order to improve our understanding of the crustal structure of the Tethyan Himalaya. We identify multiple *P*- and *S*-wave wide-angle reflections within the crystalline crust and from the Moho, but cannot identify any refracting waves beneath the Moho. We model the structure of *P*- and *S*-wave velocity throughout the whole crust, while acknowledging the significant uncertainties that are inherent in many places. A low-wave speed cover sequence may be identified with the Tethyan sedimentary cover ($Vp <$ 5.8 km s^{-1}), from the surface to a depth of (typically) 5–10 km, which is only absent where the profile crosses the Kangmar Dome. It may be presumed that these sedimentary rocks overlay a felsic upper-crustal basement (5.8 $< Vp <$ 6.3 km s^{-1}), which in places extends as far down as 35 km, and which itself overlays a 5–10-km-thick mid-crustal low-velocity zone. Between a depth of 30 and 45 km at the base of the low-velocity zone and the Moho at a depth of ∼73 km, the observed velocities gradually increase from 6.2 to 6.8 km s^{-1}. The low-velocity layer (LVL) may consist of a partial melt due to the high geothermal gradients found in the felsic rocks, or of a fluid-rich shear zone as in the ductile channel of a channel flow model. The difference in depth of the LVL between the western (central Tethyan Himalaya) and eastern segments (nearly along the STDS) at the boundary of the Dingye-Mabjia fault, leads to a north–south dip estimate of the LVL of 8.5°, which is consistent with the estimated dip of the MHT obtained from the INDEPTH-I project, and can support the channel flow model. This north–south low dip angle of subduction slab, supports that the subducting Indian lithosphere endured a transition from steep subduction to low-angle subduction, and the subduction slab flattening may be attributed to the break-off of Indian lithosphere slab beneath the Indur-Zurpo suture.

Key words: Controlled source seismology; Continental tectonics: compressional; Crustal structure; Asia.

1 INTRODUCTION

The Tibetan plateau was formed by the successive accretion of several continental blocks to the south of Eurasia, and is crossed by at least three major west–east suture zones. The most southerly of these, the Palaeocene Yarlung-Zangbo suture (YS) zone, which is marked by a discontinuous ophiolite belt over a distance of 1500 km, separates the Indian Plate and the Tethyan Himalaya to the south from the Lhasa terrane to the north. Continental collision along the YS has thickened the crust in the Himalayas and Tibet to around double that of the normal continental crust and has led to the formation of the Tibetan plateau (Tapponnier & Molnar 1977; Searle 1983; Allegre *et al.* 1984; Searle *et al.* 1987, 1988, 1997; Chang & Shackleton 1988; Molnar *et al.* 1993; Yin & Harrison 2000; Chen *et al.* 2010). The presence of a high-velocity shield-like mantle lid suggests that the Indian lithosphere underthrusts southern Tibet, possibly as far as the Bangong-Nujiang suture 300 km to the north of the YS (Owens & Zandt 1997).

The Sino-French Tibet seismic program was established in the 1980s in order to examine variations in crustal structure between the Himalaya and the Bangong-Nujiang suture. During this program, a west–east wide-angle seismic reflection/refraction profile in the Tethyan Himalaya was acquired between Peigu Tso (PGT) and Pumoyong Tso (PMYT) (Fig. 1; Tso is Tibetan for lake), and this

© 2010 The Authors
Journal compilation © 2010 RAS

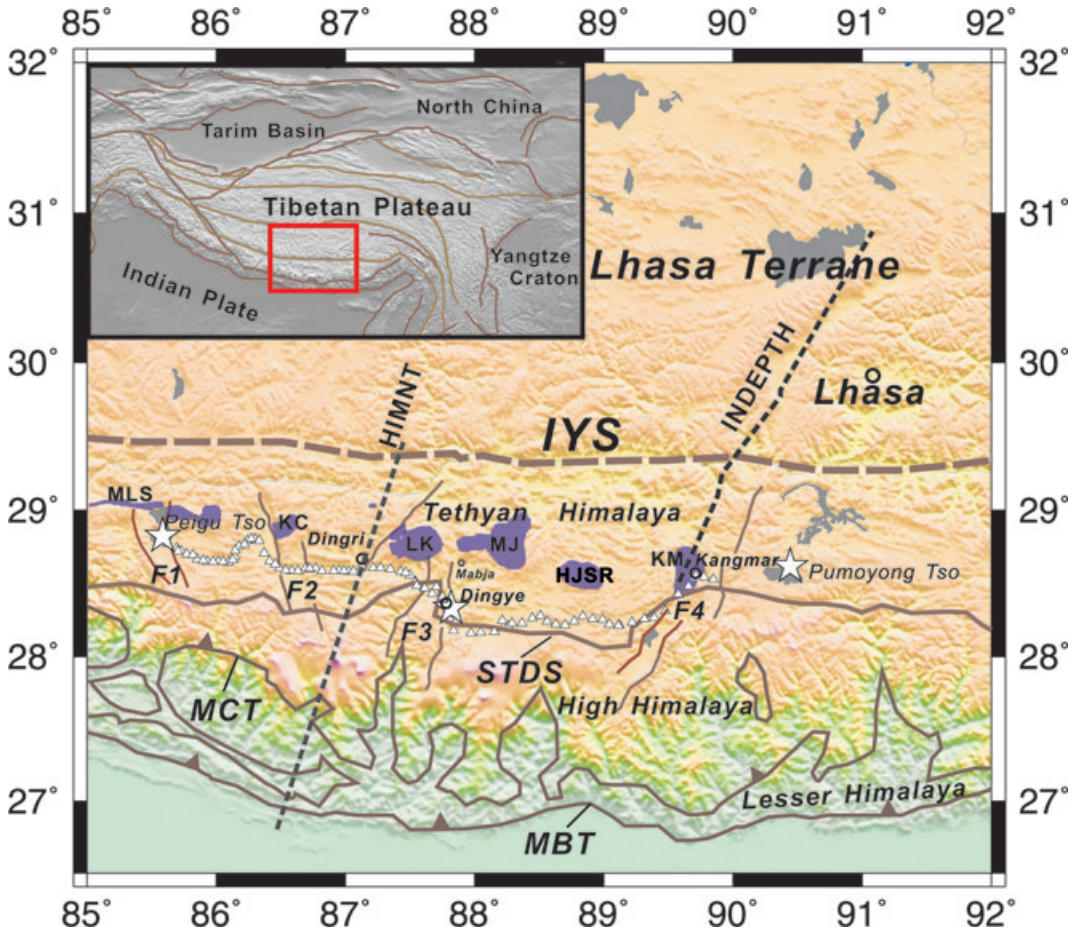

Figure 1. Location map of Southern Tibet (Alsdorf *et al.* 1998; Schulte-Pelkum *et al.* 2005). IYS: Yarlung-Zangbo suture; STDS: Southern Tibetan Detachment System; MLS: Malashan Dome; KC: Kuncuo Dome; LK: Largri-kangri Dome; MJ: Mabja Dome; HJSR: Hajinsangre; KM: Kangmar Dome; F1: Peigu Tso fault; F2: Luoza-Dingri; F3: Dinggye-Mabjia fault; F4: Yadong-Gulu fault. MBT: Main Boundary Thrust; MCT: Main Central Thrust White stars and triangles: shots and receivers of west–east wide-angle seismic profile between Peigu Tso and Pumuyong Tso. North–south profiles are represented by dashed lines. West: HIMNT passive seismic profile (Schulte-Pelkum *et al.* 2005); east: INDEPTH-I and II near-vertical reflection profiles (Alsdorf *et al.* 1998) and coincident wide-angle (Makovsky *et al.* 1996, 1999) and passive seismic (Yuan *et al.* 1997) recording along Yadong cross structure (or Yadong rift system).

forms the subject of this paper, together with data from a south–north fan and a west–east profile in the northern Lhasa terrane (Zhang & Klemperer 2005). Average 1-D crustal velocity models were obtained for the Tethyan Himalaya (Hirn & Sapin 1984; Hirn *et al.* 1984a,b,c; Sapin *et al.* 1985; Xiong *et al.* 1985; Gao *et al.* 1991), but we herein reinterpret the same data using 2-D methods in order to identify any variations in the direction of the strike. An along-strike profile that lies entirely within the Tethyan Himalaya offers the best opportunity to compare the west–east crustal structure of southernmost Tibet with the results provided by the numerous seismic profiles that have been recorded in the cross-strike, north–south direction, including wide-angle controlled-source (Hirn *et al.* 1984a; Makovsky *et al.* 1996, 1999), near-vertical controlled-source (Zhao & Nelson 1993; Brown *et al.* 1996), and teleseismic profiles (Kind *et al.* 1996; Hirn *et al.* 1997; Yuan *et al.* 1997; Schulte-Pelkum *et al.* 2005). Furthermore, because our understanding of the north–south tectonic assembly of Tibet has become much clearer in recent years (Owens & Zandt 1997; Yin & Harrison 2000; Klemperer 2006), it has become more important to resolve the lateral ambiguity inherent in the two possible models of a traditional thrust belt (Srivastava & Mitra 1994; DeCelles *et al.* 2001) and crustal flow (Clark & Royden 2000; Haines *et al.* 2003; Beaumont *et al.* 2004, 2006; Zhang & Klemperer 2005; Klemperer 2006) at the main collision belt. This ambiguity is similar to that afforded by the models of lateral tectonic escape (Tapponnier *et al.* 1982; Wang *et al.* 2008; Zhang *et al.* 2009), mid/lower crust channel flow (Clark & Royden 2000; Klemperer 2006) and lateral/vertical flowing escape (Zhang *et al.* 2010) at the eastern margin of East Tibet. In the traditional thrust belt model, the large-scale collision-parallel shortening and deformation of the Himalaya are accommodated by brittle faulting and folding in the upper crust, and localized ductile shear zones in the lower crust (Srivastava & Mitra 1994; DeCelles *et al.* 2001). In the channel flow model, however (Grujic *et al.* 1996; Nelson *et al.* 1996; Beaumont *et al.* 2004, 2006; Klemperer 2006), underthrust material from the subducting Indian Plate undergoes partial melting and returns towards the surface in the form of mid-crustal flow towards the thinner, lower-elevation crust of the foreland.

In the Himalaya and southern Tibet, somewhat contrasting tectonic behaviour has resulted from the continuing northward subduction of the Indian lithosphere that has been occurring ever since the continental collision at 57 Ma (Leech *et al.* 2005). The crustal thickening that has occurred as a result of the underthrusting of India northwards beneath the Main Himalayan Thrust (MHT)

(Zhao & Nelson 1993) has been accompanied by crustal thinning that has been accomplished both by north–south extension across the east–west South Tibetan Detachment System (STDS) (e.g. Burchfiel & Royden 1985; Burchfiel *et al.* 1992) and by east–west extension across a series of north–south trending grabens (e.g. Armijo *et al.* 1986; Chen *et al.* 1990; Fig. 1). The predominantly early-to-middle Miocene, north-dipping, low-angle STDS (Burg & Chen 1984; Burchfiel *et al.* 1992; Hodges *et al.* 1992; Ratschbacher *et al.* 1994; Coleman & Hodges 1995; Harrison *et al.* 1995) has been interpreted both in terms of a roof fault that allows ductile extrusion of a single wedge during the growth of a critical-taper orogenic thrust belt, and as the upper boundary of a long-lasting channel flow that is causing the extrusion of the Greater Himalaya Sequence (GHS) of high-grade metamorphosed Indian basement from beneath the interior of Tibet (England & Molnar 1993; Nelson *et al.* 1996; Beaumont *et al.* 2004). The Pliocene-to-Recent north–south grabens are widely believed to result from the gravitational collapse of the overthickened Tibetan crust (Molnar & Tapponnier 1978; England & Houseman 1988; Molnar *et al.* 1993) above a low-viscosity middle and lower crust (Masek *et al.* 1994), though Yin (2000) has argued that the whole of the crust and the mantle lithosphere have been involved in this extension. The High Himalaya is bounded to the south and north by the Main Central Thrust and the STDS, and the Tethyan Himalaya by the STDS and the Yarlung-Zangbo suture (Fig. 1). The Tethyan Cambrian-to-Eocene miogeoclinal sedimentary sequence, which is deposited on the passive northern margin of the Indian continent, is deformed in a complex manner, but is only slightly metamorphosed, and the STDS separates this from the underlying GHS of high-grade metamorphosed Indian basement (Gansser 1964; Le Fort 1975). The North Himalayan gneiss domes of southern Tibet consist of a series of isolated domes that provide a window through the Tethyan sequence into the GHS crystalline basement (e.g. Patiño Douce & Harris 1998; Lee *et al.* 2004). The phenomenon of uplift of these gneiss domes has been linked to a variety of possible mechanisms, including diapirism (Inger & Harris 1993; Lee *et al.* 2000, 2004; Teyssier & Whitney 2002; Zhang *et al.* 2004) and/or channel flow in the mid-to-lower crust (Beaumont *et al.* 2004, 2006; Klemperer 2006).

The Sino-French wide-angle seismic profile discussed herein lies within the Tethyan Himalaya and runs to the north of the STDS and to the south of the gneiss domes (Malashan, Kunco, Largrikangri, Mabja, Hajinsangre and Kangmar domes), and crosses the north–south trending graben systems (Peigu Tso graben; Luoza-Dingri graben; Dinggye-Mabjia graben and Yadong-Gulu graben, F1–F4 on Fig. 1, respectively). Because India is subducting northwards beneath this region, a vertical crustal cross-section should reveal the Tethyan sedimentary sequence and the occurrence of the GHS above the MHT, and the lower half of the cross-section should be found to consist of underthrusting Indian cover and basement rocks. Although the Sino-French wide-angle profile was recorded before the development of much of the tectonic theory that is now so widely accepted, and before the availability of recording equipment capable of carrying out crustal imaging at a sufficiently high spatial resolution, this wide-angle seismic profile nevertheless offers the opportunity to reveal the depth and characteristics of the MHT beneath the Tethyan Himalayan block, and to assess the proposed origins of the north–south trending faults and the North Himalayan gneiss domes. In order to attempt this assessment, the *P*- and *S*-wave data from the Sino-French experiment have been re-sampled and reinterpreted in order that the structure of the *P* and *S* waves can be remodelled.

2 PREVIOUS SEISMIC INTERPRETATIONS OF THE TETHYAN HIMALAYA

2.1 The Peigu Tso–Pumoyong Tso profile

The wide-angle seismic profile that was acquired during the joint Sino-French program of 1981 extends for a distance of 480 km from Peigu Tso (PGT) to Pumoyong Tso (PMYT), and passes through Dingye (DY), near Mabja, Kangmar (Hirn *et al.* 1984a; Teng *et al.* 1985, Fig. 1). Because only 60 analogue magnetic-tape recorders were available for the in-line experiment (45 French three-component instruments and 15 Chinese vertical-component instruments), all the shots were repeated with the recorders being located at different offsets (Teng *et al.* 1985; Gao *et al.* 1991). In total, eight large shots were fired at the three shot-points. Borehole sources were triggered twice at DY (3600 and 8000 kg), and lake shots were triggered at PGT four times (2000, 2800, 8000 and 4000 kg) and at PMYT twice (5000 and 10000 kg). Even these large shots did not propagate very well through the thick, young Tibetan crust, and as a result, the maximum useful source–receiver distance was no more than 300 km, despite attempts to record along the full profile. A world timing system was used in this experiment to provide precision in absolute timing. Neither the reliability of the instruments used, nor the retrieval of the data recorded, were as good in 1981 as they are today, and a total of only about 130 useful seismic traces were obtained, distributed over the three shot-records (Figs 2–4) at a spacing of the traces of 4–7 km.

As a result of the rather limited data set, the preliminary interpretations yielded only a single 1-D model for the entire profile, which had an upper-crustal velocity of $\sim$6.0 km s^{-1}, a lower-crustal velocity of $\sim$6.4 km s^{-1}, a mean crustal velocity of $\sim$6.25 km s^{-1}, and a broad, $\sim$12 km thick crust-mantle transition, at a depth of 70–82 km, above a mantle with an unusually high velocity of 8.5 km s^{-1} (Hirn *et al.* 1984a,c; Hirn & Sapin 1984). The high velocity recorded in the mantle was subsequently interpreted as representing eclogitization of the deepest portions of the underthrust Indian lower crust (Sapin & Hirn 1997). The four distinct 1-D profiles for the four data sets PGT, DY recorded to the west, DY recorded to the east and PMYT were presented by Teng *et al.* (1985) and Gao *et al.* (1991). These authors reported a 5.6 km s^{-1} low-velocity zone at a depth of $\sim$20 km from the two eastern velocity–depth (V–z) functions, and a 6.1 km s^{-1} low-velocity zone immediately above the Moho at a depth of 73–75 km, with a thickness of about 10 km in all four 1-D (V–z) models.

2.2 Subsequent seismic surveys and crustal structure-velocity data

The INDEPTH (International Deep Profiling of Tibet and the Himalaya) near-vertical and wide-angle seismic reflection profiles (dashed lines, Fig. 1) were measured along the Yadong cross structure (or Yadong rift system) in an almost south–north direction, and were acquired in 1992 and 1994 (Zhao & Nelson 1993; Edwards *et al.* 1994; Makovsky *et al.* 1996; Alsdorf *et al.* 1998; Wu *et al.* 1998). These profiles cross our west–east wide-angle seismic profile (white stars and triangles in Fig. 1). Using these, a major reflector (from MHT) that dips northwards beneath the Tethyan Himalaya as far as about 50 km south of the YS, was interpreted to be the detachment at the top of the underthrusting Indian crust (Zhao & Nelson 1993; Nelson *et al.* 1996; Makovsky *et al.* 1999). Interpretation of the INDEPTH wide-angle seismic data reveals a crustal thickness

© 2010 The Authors, *GJI*, **181,** 1247–1260
Journal compilation © 2010 RAS

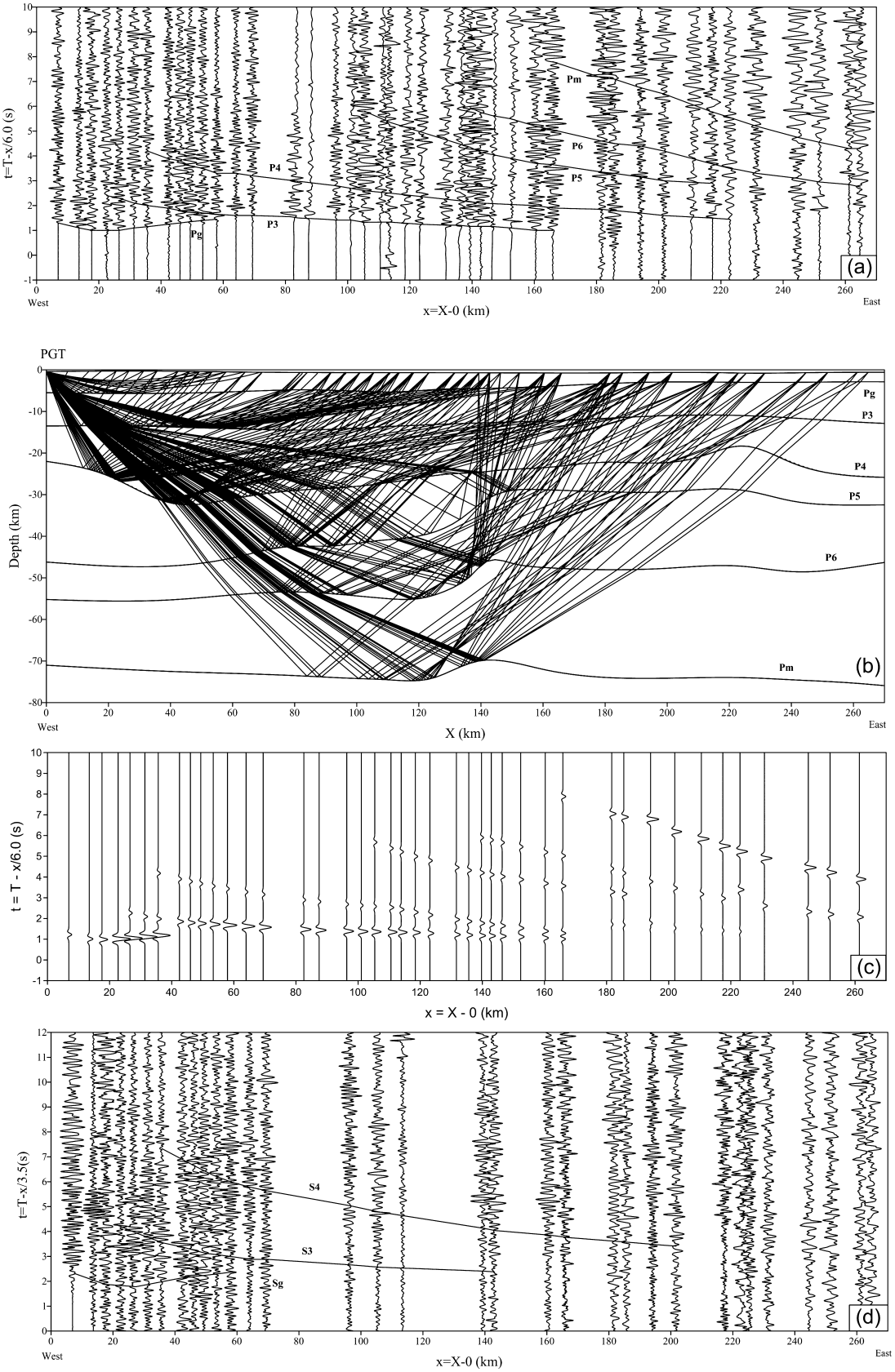

Figure 2. (a) Vertical-component wide-angle seismic profile for the two shots at Peigu Tso, filtered at 1–10 Hz and reduced by 6.0 km s^{-1}. Solid lines mark the predicted arrival times of the phases Pg, P3, P4, P5, P6 and Pm. (b) Ray diagram for the phases shown in (a); for contoured velocities see Fig. 5. (c) Synthetic wide-angle seismic gather for the shot at Peigu Tso with crustal velocity model of our final interpretation. (d) Radial-component wide-angle seismic profile for the two shots at Peigu Tso, filtered at 1–8 Hz and reduced by 3.5 km s^{-1}. Solid lines mark the predicted arrival times of phases Sg, S3 and S4.

© 2010 The Authors, *GJI*, **181,** 1247–1260
Journal compilation © 2010 RAS

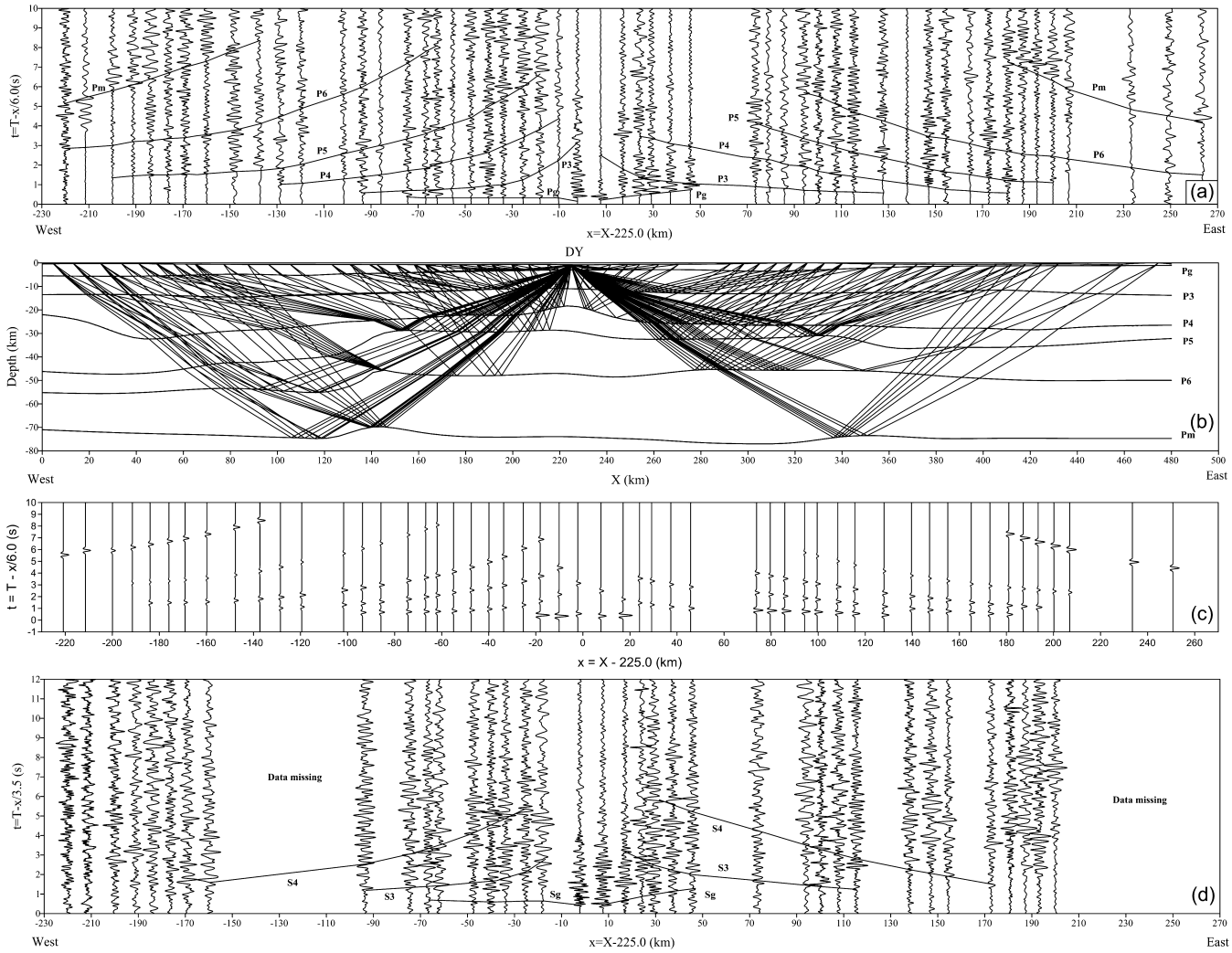

Figure 3. (a) Vertical-component wide-angle seismic profile for the two shots at Dingye, filtered at 1–10 Hz and reduced by 6.0 km s^{-1}. Solid lines mark the predicted arrival times of phases Pg, P3, P4, P5, P6 and Pm. (b) Ray diagram for the phases shown in (a); for actual velocities, see Fig. 5. (c) Synthetic wide-angle seismic gather for the shot at Dingye with the crustal velocity model of our final interpretation. (d) Radial-component wide-angle seismic profile for the two shots at Dingye, filtered at 1–8 Hz and reduced by 3.5 km s^{-1}. Solid lines mark the predicted arrival times of phases Sg, S3 and S4 from discontinuities in the upper crust. A limited total recording time for eastern stations for this shot prevented observation of *S* phases at offsets far to the east.

of about 70–75 km under the Tethyan Himalaya and a lower velocity layer (*P*-wave velocity of 5.5 km s^{-1}) about 10 km thick above the MHT (Zhao and INDEPTH group 2001)**.** Using this same wide-angle data set, Makovsky *et al.* (1996) obtained their upper crustal velocity model, which showed no low-velocity layer (LVL) above the MHT and provided no characterization of the deeper structure beneath it.

Passive seismic recording of the structure of the lithosphere and upper mantle in southern Tibet was also undertaken as part of the INDEPTH program (Yuan *et al.* 1997; Cotte *et al.* 1999). Receiver function measurements from the *P*-to-*S* converted phases show the Moho at a depth of ∼70 km and a possible increase in velocity at a depth of 35–50 km, which marks the northward dip of the MHT (Nelson *et al.* 1996). Rayleigh-wave inversions suggest a gradual increase in velocity through the lower crust beneath the Tethyan Himalaya, in contrast with a marked lower-crustal low-velocity zone in the Lhasa block north of the Yarlung-Zangbo suture (Cogan *et al.* 1998; Cotte *et al.* 1999). In 2001–2003, an areal broadband seismic network ('HIMNT') operated in Nepal and southern Tibet, across the central part of our seismic profile. This network yielded a common conversion point (CCP) image in the crust and upper mantle, where the reflection at a depth of about 40 km under the Tethyan Himalaya was interpreted as a seismic response from the MHT (Schulte-Pelkum *et al.* 2005). At the locations where the HIMNT and INDEPTH images intersect our wide-angle seismic profile, the MHT may be interpreted at depths of ∼40 and ∼32 km, respectively (Alsdorf *et al.* 1998; Zhao & INDEPTH group 2001; Schulte-Pelkum *et al.* 2005). The best-fitting 1-D velocity model obtained from earthquake relocation in the HIMNT area is given by $Vp = 5.8$ km s^{-1} ($Vs = 3.5$ km s^{-1}) above a depth of 40 km, and $Vp = 6.9$ km s^{-1} ($Vs = 4.0$ km s^{-1}) from 40 km down to the Moho at 70 km (Monsalve *et al.* 2006).

3 RE-ANALYSIS OF THE PGT-PMYT PROFILE

All previous analyses of the PGT-PMYT profile made use of 1-D models and using only the *P* waves. We herein describe the use of 2-D ray tracing to fit the observed traveltimes of a range of

© 2010 The Authors, *GJI*, **181,** 1247–1260
Journal compilation © 2010 RAS

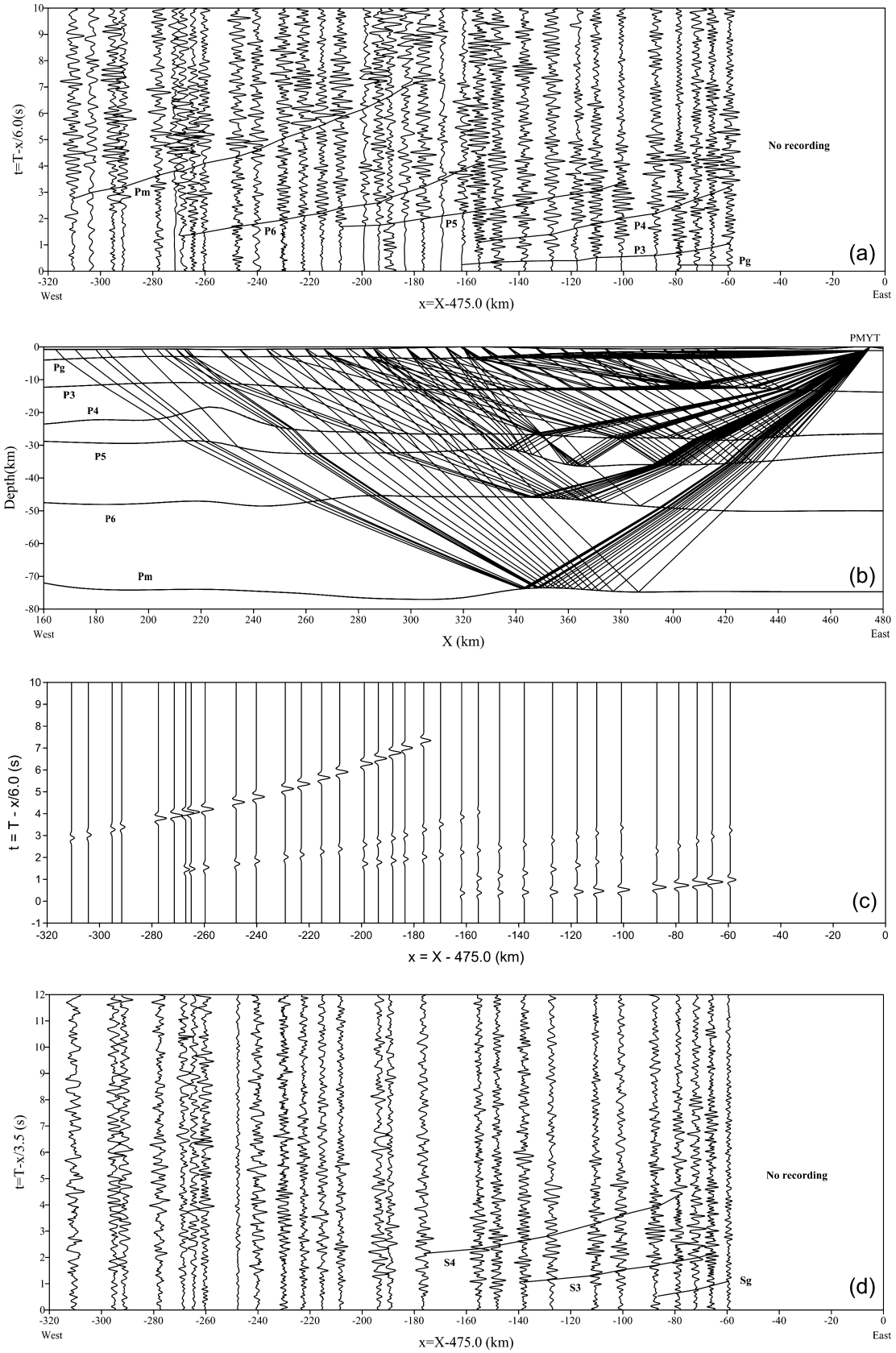

Figure 4. (a) Vertical-component wide-angle seismic profile for the shot at Pumoyong Tso, filtered at 1–10 Hz and reduced by 6.0 km s^{-1}. Solid lines mark the predicted arrival times of phases Pg, P3, P4, P5, P6 and Pm. (b) Ray diagram for the phases shown in (a); for actual velocities, see Fig. 5. (c) Synthetic wide-angle seismic gather for the shot at Pumoyong Tso with crustal velocity model of our final interpretation. (d) Radial-component wide-angle seismic profile for the shot at Pumoyong Tso, filtered at 1–8 Hz and reduced by 3.5 km s^{-1}. Solid lines mark the predicted arrival times of phases Sg, S3 and S4.

© 2010 The Authors, *GJI*, **181,** 1247–1260
Journal compilation © 2010 RAS

wide-angle compressional phases, and we have also attempted to model the shear waves. We resampled the seismic data using a sampling interval of 10 ms, and created 80-s traces. In order to enhance the signal-to-noise ratio, we used a 1-to-10 Hz bandpass filter for the *P*-wave section and a 1–8 Hz bandpass filter for the shear wave section. Furthermore, in order to produce the wide-angle seismic sections shown here, we also applied a reduction velocity of 6.0 km s^{-1} to the vertical-component traces for the *P*-wave sections (Figs 2a, 3a and 4a) and 3.5 km s^{-1} to the radial-component traces for the *S*-wave sections (Figs 2c, 3c and 4c). These reduction velocities were selected in order that the *P* and *S* phases would have similar arrival times if $Vp/Vs = 1.71$, which is equivalent to a Poisson's ratio of 0.24.

In the first stage of our model, we inverted the selected traveltime-offset curves for laterally homogeneous, layered media, in order to derive the 1-D *P*-wave velocity structure for PGT, DY-west, DY-east and PMYT using the T-square-X-square method. These four 1-D crustal velocity models were then combined to give a 2-D velocity model in which the refractor depths and *P*-wave interval velocities were adjusted to give a good fit to the traveltimes obtained using 2-D ray tracing (Figs 2b, 3b and 4b), and in which the predicted locations of the largest amplitudes (the critical distance) obtained from synthetic seismograms (Figs 2c, 3c and 4c) also matched the observations (Červený *et al.* 1977). In the conventional interpretation of deep seismic data, interfaces are generally considered to be abrupt discontinuities. In reality, these interfaces are probably characterized by a range of different velocity gradients. In this study, we almost exclusively interpreted reflection phases using interfaces with significant velocity gradients, and the main information derived from these are the depths of the interfaces and the average velocities. In the seismic sections, compressional phases are generally visible at source–receiver distances of up to 250 km (PGT, DY, Figs 2 and 3), and sometimes in excess of 300 km (PMYT, Fig. 4). From the reduced *P*-wave shot gathers, we identified six phases, denoted by Pg (through sedimentary basins and shallow crystalline basement), P3, P4, P5 and P6 (corresponding to wide-angle reflections/turning rays that penetrated successively deeper into the crust) and Pm (for the Moho reflection, Figs 2a, 3a and 4a). Pg, P4 and Pm may clearly be seen in all three record sections; P5 and P6 are less clear, particularly in the PGT and PMYT gathers, so we have less confidence in these parts of the velocity model. The prevailing frequency is 3–7 Hz for the shot PGT and 2–5 Hz for the shots DY and PGYT. The *P*-wave velocities were allowed to vary both vertically and laterally between the six reflectors that we assumed to be continuous in our scheme, but these reflectors may have represented different lithological boundaries in different locations.

Having obtained the *P*-wave velocity, we fitted the *S*-wave data (the events Sg, S3 and S4 in Figs 2d, 3d and 4d) by adjusting the *S*-wave velocities in the upper crust, but not the reflector depth. The signal-to-noise ratio of the *S*-wave data (Figs 2d, 3d and 4d) was much poorer than that of the *P*-wave data (Figs 2a, 3a and 4a). In order to identify the intracrustal *S*-wave reflections, we calculated the expected *S*-wave traveltimes using our final crustal *P*-wave velocity model with $Vp/Vs = 1.73$ and found that (1) the observed phases Sg, S3 and S4 lagged the predicted values, and hence Vp/Vs must be greater than 1.73 in order to fit the observations (Figs 2d, 3d and 4d); (2) phases S5, S6 and Sm (corresponding to P5, P6 and Pm) could not be identified with any confidence and are not shown in Figs 2d, 3d and 4d. Hence, after we had interpreted the structure of the entire crustal *P*-wave velocity, we only analysed shear wave velocity and Vp/Vs distribution in the upper crust, as constrained by the shear wave phases Sg, S3 and S4.

Figs 2(a), 3(a) and 4(a) show the comparison between the observed *P*-wave data, the calculated traveltimes, and the corresponding *P*-wave ray paths, at shots PMYT, PGT and DY, respectively. Figs 2(d), 3(d) and 4(d) show the comparison between the observed *S*-wave data of upper crust and the calculated traveltimes. These figures show only those parts of the model space that are illuminated by the shot points for each shot section. In Fig. 5, we show the final results of our interpretation of the PGT-PMYT profile, including the ray coverage (Fig. 5a) of this wide-angle seismic experiment, crustal *Vp* (Fig. 5b), upper-crustal *Vs* (Fig. 5c) and Vp/Vs ratio (Fig. 5d) models. As in all crustal refraction surveys, both the velocities and depths for specific reflectors are subject to some degree of uncertainty; thus, we here focus only on those phenomena that can be interpreted with more confidence and that are clearly related to the major structures that were identified previously.

The best test of the validity of the final models is whether the predicted traveltimes of the *P* and *S* waves (*P*: solid lines in Figs 2a, 3a and 4a; *S*: solid lines in Figs 2d, 3d and 4d) match those of the visible phases adequately. For many of the late-arriving phases, considerable uncertainty is inherent in the selection of the arrival times (up to 0.5 s). The average crustal *P*-wave velocity is about 6.2 km s^{-1}, and the crustal depth is about 73 km along the PGT–PMYT profile. The critical distances of the three shot gathers (Figs 2–4) are about 150 km (i.e. twice the crustal thickness). The propagating lengths of the Pm ray path are about three times the crustal thickness (i.e. ∼220 km, corresponding to a traveltime of 220 km/6.2 km s^{-1}, or about 35.5 s). An error of 0.5 s in Pm traveltime corresponds to an uncertainty in velocity of the order of about 0.09 km s^{-1} ($\approx 220\,\mathrm{km}/36\,\mathrm{s} - 6.2\,\mathrm{km\,s^{-1}} \approx 0.09\,\mathrm{km\,s^{-1}}$), which is equivalent to variations in the crustal structure of about 3 km ($\approx \pm 0.5\,\mathrm{s} \times 6.2\,\mathrm{km\,s^{-1}} \approx \pm 3\,\mathrm{km}$). Fig. 5(a) shows the effective shot gather-coverage generated by this experiment, using the final model. Due to the fact that only three shot points are used, a maximum of three crossing shot gathers is possible at any point in the model, and in fact is only achieved in its central section. Wherever two shot gathers cross over, in principle we may resolve the true rock velocity from the apparent velocity independently, as a result of the structural dip. Where only one ray path crosses a region, considerable uncertainty is inherent in the apparent velocity, but in practice if a wide-angle phase is continuous throughout the recorded section, the actual velocities and reflector geometries are likely also to vary smoothly. Nevertheless, the extreme lateral continuity of our crustal layers is an artefact of our somewhat limited ray coverage and our modelling technique, and we are unable to determine whether lateral transitions in velocities and thicknesses are abrupt or transitional, from the seismic data obtained. Where no rays traverse a region, there are no constraints on the velocities, and in our final summary models (Figs 5b–d) we have left these regions blank.

In the remainder of this section, we focus on the interpretation of, and the implications of, the best-constrained crustal sections, located at a distance of 80–150 km along the profile (beneath Dingri) and at a distance of 340–390 km along the profile [below and to the west of Kangmar Dome (KM)], where ray coverage is reversed at the Moho. Beneath a generally thin sedimentary cover, the crust may be crudely divided into an upper crust ($5.8 < Vp < 6.3$ km s^{-1} extending to a depth ranging from ∼20 to 35 km), above a LVL modelled as ∼10 km thick, in which the velocities are reduced to ∼5.8 km s^{-1}, and a lower crust (depths below ∼30–45 km, $6.2 < Vp < 6.8$ km s^{-1}).

Pg and Sg are visible down to a offset of about 60–80 km in the three shots (Figs 2a,c, 3a,d and 4a,d), and have clearly different traveltimes in the different record sections. In the western (PGT)

© 2010 The Authors, *GJI*, **181,** 1247–1260
Journal compilation © 2010 RAS

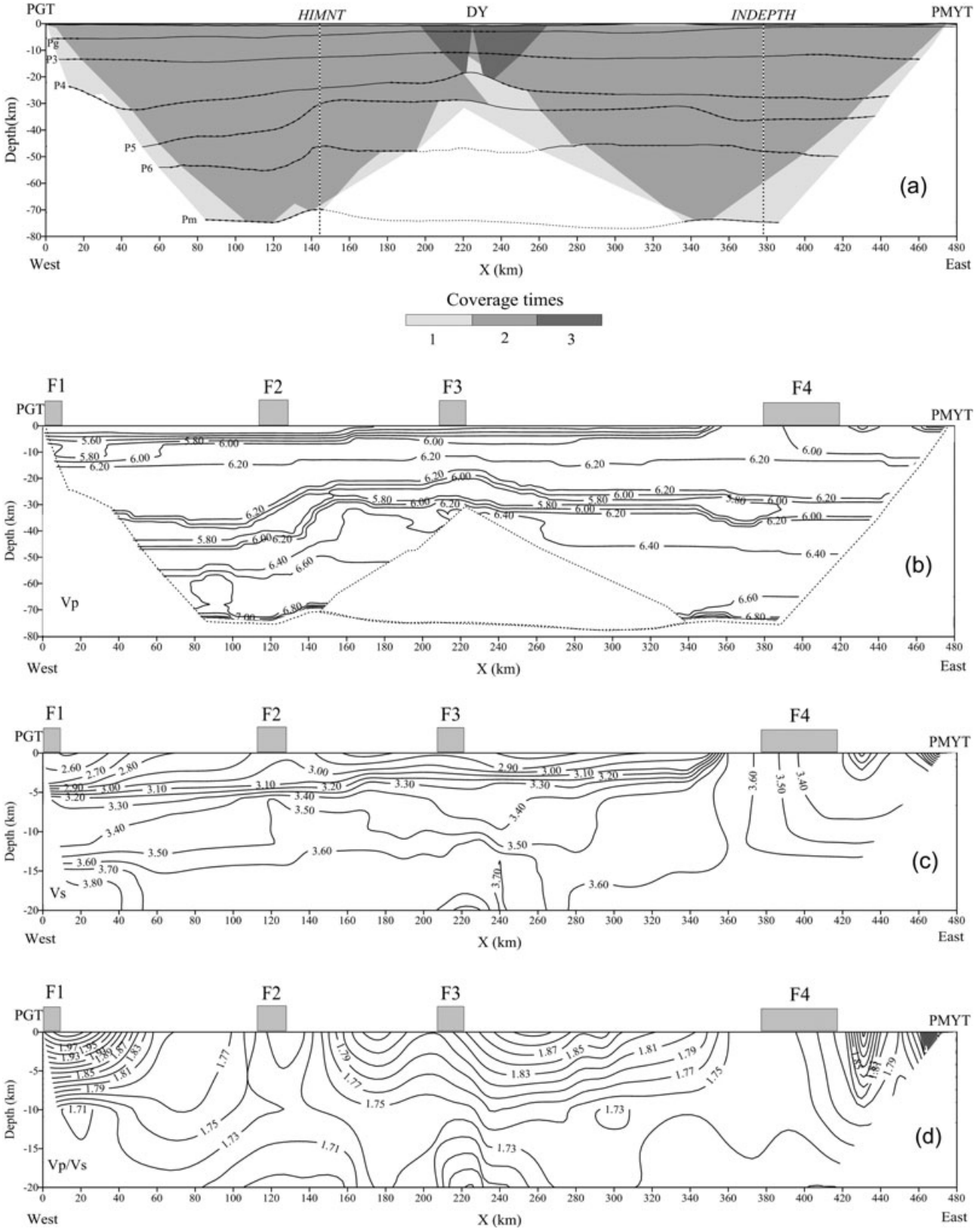

Figure 5. 2-D crustal structure interpreted along the Peigu Tso-Dingye-Pumoyong Tso profile. (a) Summary shot coverage composited from ray-trace models in Figs 2(b), 3(b) and 4(b); regions of the model with reversed coverage (two or three shots) are denoted by darker shading; regions that are unreversed are denoted by lighter shading; unconstrained regions are blank. (b) *P*-wave velocities (in km s^{-1}); note that the layer boundaries tend to lie along regions of large vertical gradients in velocity, but are not iso-velocity boundaries. (c) *S*-wave velocities (in km s^{-1}) of the upper crust constrained by events Sg, S3 and S4; note that the layer boundaries tend to lie along regions of large vertical gradients in velocity, but are not iso-velocity boundaries. (d) *Vp*/*Vs* ratio (with a contour interval of 0.02) of the upper crust determined as the ratio of the velocities in (b) and (c).

© 2010 The Authors, *GJI*, **181,** 1247–1260
Journal compilation © 2010 RAS

shotpoint, Pg is clearly delayed by ∼1 s with respect to the equivalent phase from the central and eastern shots (DY and PMYT) (Xiong *et al.* 1985). We presume that this corresponds to a greater thickness of sedimentary rocks beneath Peigu Tso and the F1 graben; in this region of our model, velocities ≤5.8 km s^{-1} extend to a depth of ∼12 km, which is twice as deep as elsewhere along our profile. Unfortunately, the spacing of the stations on our seismic profile is too sparse for us to detect the sedimentary basins associated with the Neogene grabens that cross our profile and prevents anything more than speculation about the relationship between their bounding faults and the deeper crustal structure.

Beneath the sedimentary basins, the upper crust is characterized by low vertical velocity gradients and a low-velocity zone at its base. The events P3, S3 and P4, S4, which are visible over offset ranges of ∼30–150 and ∼40–220 km from each shot, are modelled as reflected *P* and *S* waves from upper-crustal interfaces in the depth range 12–30 km. Although reversing rays from pairs of shot-points help to constrain the velocities in this depth range to ∼5.8–6.2 km s^{-1} (*Vp*) and 3.4–3.8 km s^{-1} (*Vs*), the wide-angle reflecting points are not reversed (Fig. 5a). Our inability to identify clear crossover between P3 and P4 (e.g. PMYT record section, Fig. 4a) suggests the prevalence of low vertical velocity gradients, even local low velocity zones, in these layers. We formally model only one low-velocity zone, between P4 and P5. On both the PMYT (Fig. 4a) and the DY (to the west, Fig. 3a) record sections, there is a clear time gap between the point at which P4 is last observed and where P5 appears, which indicates the presence of a hidden layer. This behaviour is even more pronounced on the PGT record section (Fig. 2a), which suggests that the low-velocity zone is more marked in the west. The thickness and velocity of the interpreted LVL are not well resolved, but the data suggest that the base of the layer, i.e. the base of the felsic upper crust, is at 29–35 km and is somewhat deeper in the west than in the east. The average *P*-wave velocity from the surface to the base of the upper crust is 5.9–6.0 km s^{-1}. Low-velocity zones occur naturally in a granitic crust that has a high geothermal gradient (Min & Wu 1987; Christensen 1996), without the need for partial melting. However, the evidence elsewhere in the Himalayan block for partial melt in the upper crust (Nelson *et al.* 1996; Hirn *et al.* 1997; Makovsky & Klemperer 1999) suggests that our low velocity zone may also mark a high-temperature region where partial or incipient melting may occur.

Event P6 is a clear arrival on the DY record section (Fig. 3a), from 160–210 km to the west and 210–250 km to the east (in each case the maximum observed offset is limited by the maximum recording offset). P6 is also clearly visible on the PGT record section (Fig. 2a), at offsets from 160 to 270 km. The modelled reflector lies at a depth of 45–55 km (somewhat deeper in the east than in the west) and the average *P*-wave velocity from the surface to the base of this layer is 6.1–6.2 km s^{-1}. The lower crust (in which the *P*-wave velocities do not exceed 6.6 km s^{-1}) must also be composed of felsic to intermediate material (Christensen & Mooney 1995). Any mafic component of the underthrust Indian crust must now be in eclogite facies beneath the seismic Moho.

Event Pm has the largest amplitude but the lowest frequency (1–4 Hz) (hence it is the most reverberative and hardest to identify precisely), and is interpreted to be a reflection from the Moho. The critical offset is between about 180 and 220 km. There is no obvious change in crustal thickness between the west and the east of the profile, in that the Moho depth is about 70–73 km beneath the Kuncuo dome and 72–75 km near the Kangmar dome. The traveltimes for receivers in the eastern part of the profile (DY-east and PMYT) are very similar at equivalent offsets to those in the western part of the profile (PGT and DY west). The average crustal *P*-wave velocity is 6.2–6.3 km s^{-1}

4 DISCUSSION

4.1 Comparison with related studies: Moho depth and crustal velocity

Our interpreted crustal thickness of 70–75 km is consistent both with other independent data sets (Chun & Yoshii 1977; Kind *et al.* 1996; Rodgers & Schwartz 1997; Yuan *et al.* 1997; Galve *et al.* 2002) and previous interpretations of the wide-angle seismic profile described herein (Hirn & Sapin 1984; Xiong *et al.* 1985; Gao *et al.* 1991).

The Moho depth obtained using our final model also shows good correspondence with the seismic reflector, having a 22 s two-way traveltime obtained using the deep seismic reflection data from the INDEPTH project (Zhao *et al.* 1996; Alsdorf *et al.* 1998). The crustal thickness beneath our wide-angle seismic profile appears to be somewhat uniform in nature, which contrasts rather markedly with the more obvious lateral variation in crustal thickness (>10 km change in thickness) obtained from a west–east wide-angle seismic profile of a similar length in the northern Lhasa terrane (Zhang & Klemperer 2005). The strength of the subducting Indian crust may mitigate against orogen-parallel changes in crustal thickness in the Tethyan Himlaya, whereas a very weak lower crust in the Lhasa terrane may permit significant changes in crustal thickness.

At Kangmar, our west–east seismic profile crosses the Yadong cross structure and intersects the nearly orthogonal INDEPTH seismic profile (Makovsky *et al.* 1999; Zhao & the INDEPTH group 2001, Fig. 1). In the model of Makovsky *et al.* (1999), the *P*-wave velocity increases from 5.5 to 5.8 km s^{-1} from the surface to a depth of 5 km, then increases from 6.0 to 6.2 km s^{-1} down to the MHT. The depth of the young extensional basins in the Yadong cross structure along the Common Midpoint (CMP) Profile was constrained to a maximum of 2 km (Makovsky *et al.* 1999). In the model of Zhao and the INDEPTH Group (2001), which used the same INDEPTH wide-angle seismic data set, the *P*-wave velocity was about 5.7 km s^{-1} from the surface to a depth of 12 km, and then increased to 6.2 km s^{-1} down to the top of the LVL, where the *P*-wave velocity was 5.5 km s^{-1}. This *P*-wave velocity of the LVL is 0.3 km s^{-1} slower than our 5.8 km s^{-1}. By comparing the 1-D crustal velocity columns under Kangmar dome obtained from the INDEPTH profile and shown in Fig. 6a (Zhao & INDEPTH group 2001) with our PGT-PMYT profile, we find a difference in crustal velocity between the north–south and west–east direction. From the surface to a depth of 25 km, the *P*-wave velocity along the north–south direction is apparently 0.2–0.4 km s^{-1} slower than that in the west–east direction, but at a greater depth it is about 0.2 km s^{-1} higher.

Near Dingri, our west–east seismic profile crosses the Himalaya Nepal Tibet Seismic Experiment (HIMNT) profile (Fig. 1) (Schulte-Pelkum *et al.* 2005; Monsalve *et al.* 2006). In the HIMNT experiment, Monsalve *et al.* (2006) simultaneously invert for earthquake locations, 1-D *P*- and *S*-wave velocity models, and station corrections by using (1) the *P* and *S* traveltimes obtained from local earthquakes and (2) the initial earthquake locations and the starting three-layer velocity models described by Pandey *et al.* (1999) for the Nepal area and by Cotte *et al.* (1999) for south Tibet. In their final three-layer velocity model for south Tibet, from the surface to a depth of 35 km, the *P*-wave velocity is 5.8 km s^{-1}, but then increases to 6.9 km s^{-1} from there to a depth of 70 km. In the upper

© 2010 The Authors, *GJI*, **181,** 1247–1260
Journal compilation © 2010 RAS

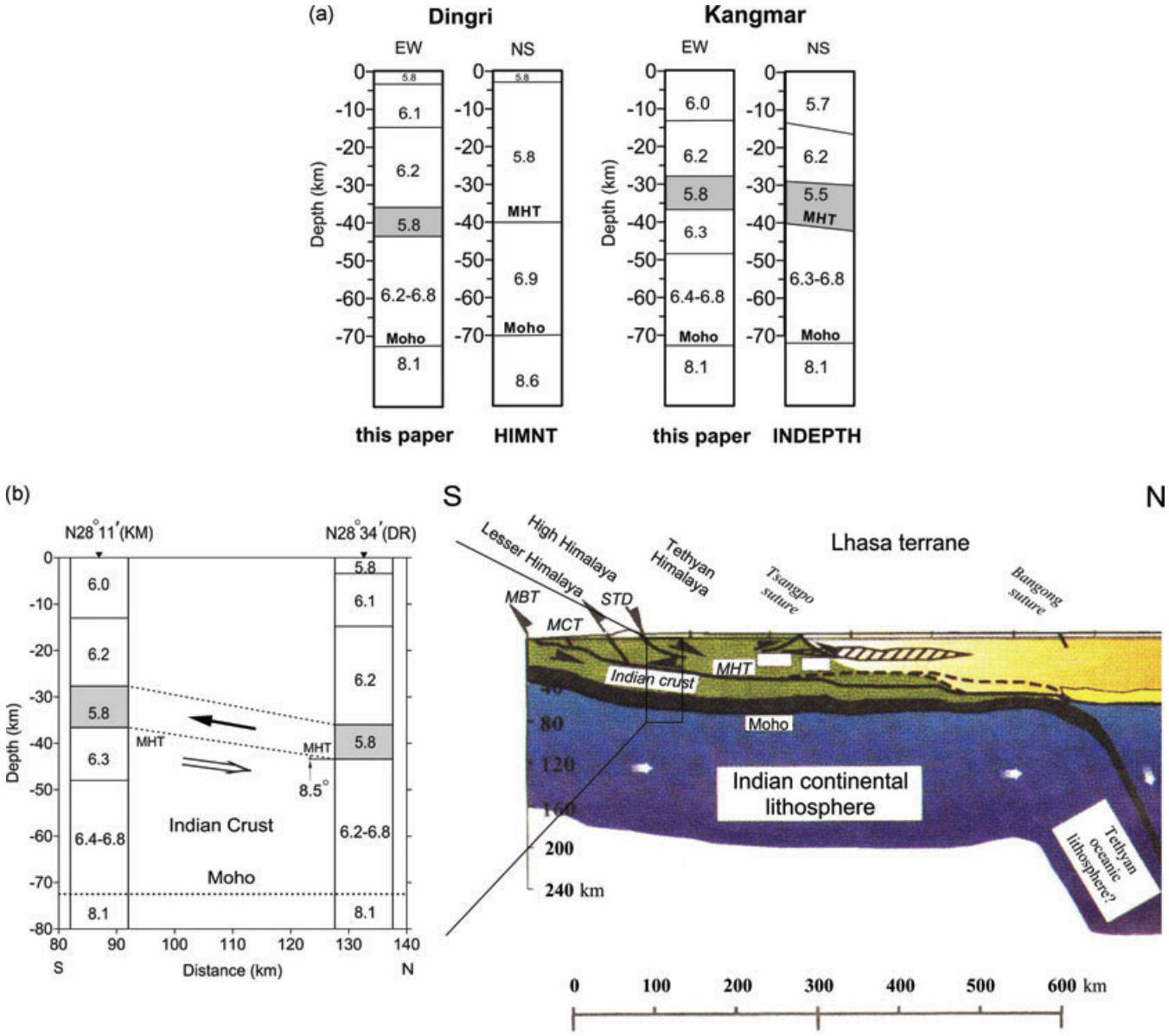

Figure 6. (a) Comparison of *P*-wave velocity–depth columns of the crust under Kangmar (Zhao & INDEPTH group 2001; Monsalve *et al.* 2006; Zhang and Klemperer, this study; left-hand panel) and Dingri (Schulte-Pelkum *et al.* 2005; Monsalve *et al.* 2006; Zhang and Klemperer, this study; right-hand panel). (b) Right-hand panel: cartoon map showing the subduction of Indian lithosphere under Himalaya and the probing crustal portion of the profile (after Owens & Zandt 1997); Left-hand panel: the LVL dip from the LVL depth difference between Kangmar and Dingri is estimated to be about 8.5°, similar to the figure of 7.5° obtained from the INDEPTH-I wide-angle seismic profile (Makovsky *et al.* 1996).

mantle (>70 km), the *P*-wave velocity is 8.6 km s^{-1}. By comparison with our 1-D *P*-wave velocity model (Fig. 6a), the west–east profile is characterized by *P*-wave velocities that are 0.2–0.3 km s^{-1} higher than those found in the HIMNT profile for the top 40 km, and 0.1 km s^{-1} lower for the lower part of the crust (from 40 to 70 km). The most remarkable difference in *P*-wave velocity occurs at depths >70 km. Even though there is some difference of layering in the crust from these two sets of seismic data that have different vertical resolutions, the crustal models are consistent, in that they display the same intracrustal discontinuity at a depth of 40 km and at the Moho at a depth of about 70 km.

The differences in velocity obtained for the upper and lower crust that we describe above may result from uncertainties of interpretation, (compositional) seismic velocity heterogeneities, and/or seismic anisotropy from crustal deformation. Because the crustal velocity difference of 0.2–0.4 km s^{-1} between the north–south and west–east directions is —two to four times the interpretation uncertainty of about 0.09 km s^{-1}, we suggest in this case that the difference in velocity is due mainly to the lateral heterogeneity or seismic anisotropy.

Alternatively, if this discrepancy in seismic velocity is attributed to velocity anisotropy, we can calculate *P*-wave anisotropy under the Kangmar dome and in the region near Dingri, and provide constrains to understand the deformation mechanism that pertains to southern Tibet. Down to a depth of 25 km, the *P*-wave velocity is about 5.90 km s^{-1} along the west–east profile, and 5.50–5.70 km s^{-1}

© 2010 The Authors, *GJI*, **181,** 1247–1260
Journal compilation © 2010 RAS

along the nearly north–south profile (Fig. 6a), so that the *P*-wave velocity anisotropy is about 3 per cent. In a similarly way, the *P*-wave anisotropy is about 1 per cent for the middle crust, and about 6 per cent for the lower crust. By assuming the seismic structure of the upper crust from the INDEPTH-1 wide-angle seismic experiment, we obtain about a 1.5 per cent east–west extension by normal faulting across the 1000-km-wide Tethyan Himalaya (Makvosky *et al.* 1996), in agreement with the estimate of about 2 per cent made by Armijo *et al.* (1986). The seismic lithospheric imbrication images obtained from this west–east profile (Burg & Chen 1984; Burg *et al.* 1984; Hirn *et al.* 1984a,b,c; Matthews & Hirn 1984) suggest the possibility of differential thickening either side of a decoupling intracrustal decollement (Sapin & Hirn 1997). Our potential principal preference (deformation) directions from the *P*-wave velocity discrepancy in the upper, middle and lower crust do not conflict with either the channel flow model in the middle crust (Beaumont *et al.* 2004, 2006; Klemperer 2006) or the injection model of the Indian crust into the lower crust (Zhao & Morgan 1987).

4.2 The low-velocity zone above the MHT?

In our model, there is one LVL with a depth range of about 25–35 km in the east of the profile. The bottom of the LVL exhibits lateral variation in depth along the west–east profile. This lateral variation is consistent with that found in the INDEPTH profile at Kangmar (Makvosky *et al.* 1999; Zhao & INDEPTH group 2001) and in the HIMNT profile near Dingri (Monsalve *et al.* 2006). From seismic reflection (Zhao & Nelson 1993; Hauck *et al.* 1998) and wide-angle seismic profile data (Makvosky *et al.* 1999), the depth of the MHT under the southern domain of the Kangmar dome is about 25 km, and is about 30 km under the northern domain of the dome. From the HIMNT experiment, the CCP stack of the radial-component receiver function clearly shows strong reflection at a depth of about 40 km near Dingri (Schulte-Pelkum *et al.* 2005).

The depth of the LVL varies within the MHT, with strong reflection from the INDEPTH-I near-vertical seismic reflection profile under Kangmar (Zhao & Nelson 1993) and the CCP stack image near Dingri (Schulte-Pelkum *et al.* 2005). One key question relates to the relationship between the LVL and the MHT, and whether the top or the bottom of the LVL corresponds to the MHT. If the bottom of the LVL is the MHT, then the LVL is more likely to be a partial melt or a fluid-rich shear zone, like the ductile channel of the channel flow model (Beaumont *et al.* 2004, 2006; Klemperer 2006). If the top of the LVL is the MHT, then the LVL could consist of subducting Indian sediments (Zhao & INDEPTH group 2001). The alternative interpretations of the LVL in the Tethyan Himalayan include that it consists of partially melted granite (Kind *et al.* 1996; Zhao & INDEPTH group 2001), an ophiolitic slab beneath the Indian-Asian suture in southern Tibet from the mid-crustal reflector (with the presence of relatively large quantities of free aqueous fluids) (Makovsky *et al.* 1999), or a downward sliding of the Mesozoic sedimentary formation as a result of the movement of the STDS (Zhao & INDEPTH group 2001). The LVL is also consistent with the presence of a low resistivity zone obtained from magnetotelluric studies (Unsworth *et al.* 2005). The low shear wave velocity obtained from surface wave tomography implies that it is only the presence of melts or fluids that can explain both the low resistivity and low velocity in the LVL (Caldwell *et al.* 2009). In the channel flow model, the MHT tips out northwards, and the underthrust Indian upper crust is decoupled from the lower crust and accreted into the upper Asian Plate, where it is heated and progressively converted into a ductile channel (Caldwell *et al.* 2009). The analyses of granulite samples collected in the Higher Himalaya demonstrate that the emplacement of the remelting granite is closely linked with the occurrence of granulite (featured with strong shearing deformation, Liu *et al.* 2009), which may lend support to the channel flow model or to a lower crustal extrusion. In the following section, we argue that the LVL may consist of either a partial melt due to high geothermal gradients in the felsic rocks or a fluid-rich shear zone as the ductile channel of the channel flow model, but cannot consist of the sedimentary cover of the subducted Indian crust, where the LVL lies above the MHT.

In order to demonstrate our theory that the bottom of the LVL corresponds to the MHT, we (1) combine the crustal velocity model of our west–east profile with that of two other approximately north–south profiles where the INDEPTH-I and II profiles and the HIMNT profile intersect our west–east profile (Fig. 1) and (2) compare the *P*-wave velocity–depth columns of the crust under Kangmar (the two right-hand columns of Fig. 6a) and near Dingri (the two left-hand columns of Fig. 6a). From our west–east profile, beneath Kangmar the depth at the bottom of the LVL is about 30 km, which is the same as the depth of the MHT (Zhao & INDEPTH group 2001). Near Dingri, the depth at the bottom of the LVL in our profile is about 40 km, which translates into the bottom of the layer having a velocity of 5.8 km s^{-1} (Monsalve *et al.* 2006) and the MHT reflector on the CCP stack image (Schulte-Pelkum *et al.* 2005). We therefore infer that it is possible that between Dingri and Kangmar, the bottom of this LVL corresponds to the MHT from the INDEPTH-I seismic reflection section, with a single path traveltime of about 4 s (Zhao & Nelson 1993).

4.3 West–east variation of crustal structure along the PGT-PMY profile

From our final crustal models of *Vp*, *Vs* and *Vp*/*Vs* ratio (Fig. 5), it may be seen that although there is no significant variation in crustal thickness along the profile, within the crust there are nevertheless clear geometrical differences in intracrustal discontinuities with the boundary of Dingye (about 200 km along the profile). This difference may be attributed to the diversity of the responses obtained to the different tectonic units identified in the west–east seismic profile. Using Fig. 1, we can divide the profile into two segments: (i) the western segment (from the Dingye to Peigu Tso), which nearly extends along the STDS and (ii) the eastern segment (from Dingye to Pumongyong Tso) in the Tethyan Himalaya. The crustal structures of the two segments reveal a horizontal homogeneity and show that there is no significant lateral variation of crustal structure along the STDS and in the central Tethyan Himalaya. If the crustal structure of the western segment of the profile is extended in an easterly direction towards the north of the eastern segment of the profile, the difference in LVL depth between the two segments can be used to estimate the dip of the LVL. From the difference in the LVL depths between the STDS and the central Tethyan Himalaya, the LVL dip may be estimated at about 8.5° (Fig. 6b). Our estimate is roughly consistent with of the 7.5° dip of the MHT estimated by Makovsky *et al.* (1996, 1999). This is steeper than most of the basal decollements observed in the foreland of orogenic belts and fits more comfortably into the category of crustal-scale ramps that project down to the Moho in the orogenic hinterland (Cook & Varsek 1994). This consistency of north–south dip angle between the LVL and the MHT may indicate that the LVL could be the flow channel that underlies the subducting interface of the MHT.

© 2010 The Authors, *GJI*, **181,** 1247–1260
Journal compilation © 2010 RAS

It is noteworthy that the MHT can be found as a thrust 'flat' under the southern end of the INDEPTH-I reflection profile, but that the MHT reflector changes in dip under the Tethyan Himalaya (Hauck *et al.* 1998). The crustal velocity model along the Yadong-NamuTso wide-angle seismic profile shows that the MHT dips northwards at an angle of about 10° from Yadong to Kangmar (figs 7–18 of Zhao & INDEPTH group 2001). On the basis of geochemistry studies, Indian continental subduction was inferred to be at a relatively steep angle of about 55° for an earlier (about 57 Ma) steep subduction period in the Indina-Asia collision (Decelles *et al.* 2001; Leech *et al.* 2005). Our LVL dip estimation and the INDEPTH-I profile reveals the north–south variation of the LVL (and the MHT) (Fig. 6a), which demonstrates that the subducting Indian lithosphere endured a transition from steep subduction to low-angle subduction, which can be explained as the subduction slab flatting responding to breaking off of the Indian lithosphere slab beneath the Indur-Zurpo suture (Leech *et al.* 2005; Fig. 6b). The spatial and temporal changes of subduction angle of the subducting Indian lithosphere slab probably contribute to the generation of north–south trends in normal faulting and high-grad metamorphic domes (e.g. Burg & Chen 1984; Harrison *et al.* 1999; Lee *et al.* 2000, 2004; Thiede *et al.* 2006).

5 CONCLUSIONS

We have reinterpreted data obtained from the Peigu Tso-Pumoyong Tso deep seismic sounding, and have obtained the seismic structure of the crustal *P*-wave velocity model and the upper-crustal *S*-wave velocity model. We draw the following principal conclusions from the analysis of the west–east seismic refraction profile, by making comparisons with INDEPTH and HIMNT profiles in the Tethyan Himalaya, southern Tibet.

(1)The crustal thickness under the Tethyan Himalayan is about 73 km, which is consistent with the INDEPTH wide-angle seismic interpretation and the structure inferred from the HIMNT data set. There is no strong *P*-wave velocity heterogeneity and no remarkable west–east variation of crustal thickness along the PGT–PMYT profile.

(2)The bottom of the LVL exhibits lateral variation in depth along the west–east profile, and may correspond to the MHT of the INDEPTH-1 deep seismic reflection section. The LVL is more likely to be a partial melt or fluid-rich shear zone, as represented by the ductile channel in the channel flow model. The difference in LVL depth between the western (central Tethyan Himalaya) and eastern (nearly along the STDS) segments with the boundary of Dingye-Mabjia fault leads to an LVL north–south dip estimate of 8.5°, which is consistent with the dip estimate made using INDEPTH-I MHT data. This consistency of north–south dip angle between the LVL and the MHT may indicate that the LVL could be the flow channel that underlies the subduction interface of the MHT, and can lend support to the channel flow model (Beaumont *et al.* 2004, 2006; Klemperer 2006). This north–south low dip angle of subduction slab, supports that the subducting Indian lithosphere endured a transition from steep subduction to low-angle subduction (Leech *et al.* 2005), and the subduction slab flattening may be attributed to the break-off of Indian lithosphere slab beneath the Indur-Zurpo suture.

ACKNOWLEDGMENT

This work was funded by the Ministry of Science and Technology of China (Grant number 2002CB412604), the Chinese National Nature Sciences Foundation (Grant numbers 40721003 and 40830315) and the Chinese Academy of Sciences (CAS) (Grant number KZCX2-YW-132). The wide-angle seismic data were acquired by the Sino-France joint project, and resampled by Yingkang Li, Jingwei Li and Jinyi Fan of Institute 562 of the Chinese Academy of Geological Science, which is administered by the Ministry of the Land and resources of China. We acknowledge the help and suggestions from Jeffrey Lee, Jiwen Teng, Yun Chen, Shaobai Xiong, Zhouxun Yin, Zhiming Bai, Shufang Zhang, Tao Xu, Deyuan Lu and Enru Liu. We also thank I. Grevemeyer, M. Scherwath, V. Dennis, C. Ebinger and R. Hobbs for their constructive comments, which greatly improve the study and the paper presentation, and the State Key Lab. of Lithospheric Evolution and the Institute of Geology and Geophysics, CAS, for permission to publish this work.

REFERENCES

Allegre, C.J. *et al*., 1984. Structure and evolution of the Himalaya-Tibet orogenic belt. *Nature,* **307,** 17–22.

Alsdorf, D. *et al*., 1998. INDEPTH (International Deep Profiling of Tibet and the Himalaya) multichannel seismic reflection data: description and availability, *J. geophys. Res.,* **103**(B11), 26 993–26 999.

Armijo, R., Tapponnier, E., Mercier, J.L. & Tongling, H., 1986. Quaternary extension in southern Tibet: field observations and tectonic implications. *J. geophys. Res.,* **93,** 13 803–13 872.

Beaumont, C., Jamieson, R.A., Nguyen, M.H. & Medvedev, S., 2004. Crustal channel flows: 1. Numerical models with applications to the tectonics of the Himalayan-Tibetan orogen, *J. geophys. Res.,* **109,** B06406, doi:10.1029/2003JB002809.

Beaumont, C., Nguyen, M.H., Jamieson, R.A. & Ellis, S., 2006. Crustal flow modes in large hot orogens, in *Channel Flow, Ductile Extrusion and Exhumation in Continental Collision Zones*, Vol. 268, pp. 91–146, eds Law, R.D., Searle, M.P. & Godin, L., Geological Society, London, Special Publications.

Brown, L.D. *et al*., 1996. Bright spots, structure, and magmatism in southern Tibet from INDEPTH seismic reflection profiling, *Science,* **274,** 1688–1690.

Burchfiel, B.C. & Royden, L.H., 1985. North–south extension within the convergent Himalayan region, *Geology,* **13,** 679–682.

Burchfiel, B.C., Chen, Z., Hodges, K.V., Yuping, L., Royden, L.H., Changrong, D. & Jiene, X., 1992. The south Tibetan detachment system, Himalayan Orogen: extension contemporaneous with and parallel to shortening in a collisional mountain belt, *Geol. Soc. Am., Spec. Pap.* **269,** 41 pp.

Burg, J.P. & Chen, G.M., 1984. Tectonics and structural zonation of southern Tibet, China, *Nature,* **311,** 219–223.

Burg, J.P., Capais, D. & Capais, D., 1984. Deformation of the crystalline main central sheet in south Tibet (China), *J. Struct. Geol.,* **6**(5), 535–542.

Caldwell, W.B., Klemperer, S.L., Rai, S.S. & Lawrenc, J.F., 2009. Partial melt in the upper-middle crust of the northwest Indian Himalaya revealed by Rayleigh wave dispersion, *Tectonophysics*, **477,** 58–65, doi:10.1016/j.tecto.2009.01.013.

Červený, V., Molotkov, I.A. & Pšenčík, I., 1977. *Ray methods in Seismology*, University of Karlova, Prague.

Chang, C. & Shackleton, R.M., 1988. *The Geological Evolution of Tibet*, The Royal Society, London.

Chen, Y., Badal, J. & Hu, J.F., 2010. Love and Rayleigh wave tomography of the Qinghai-Tibet Plateau and surrounding areas, *Pure appl. Geophys.*, **167,** doi:10.1007/s00024-009-0040-1.

Chen, Z., Liu, Y., Hodges, K.V., Burchfiel, B.C., Royden, L.H. & Deng, C., 1990. The Kangmar ome—a metamorphic core complex in Southern Xizang (Tibet), *Science,* **250,** 1552–1556.

Christensen, N.I. & Mooney, W.D., 1995. Seismic velocity structure and composition of the continental crust: a global view, *J. geophys. Res.,* **100,** 9761–9788.

Christensen, N.I., 1996. Poisson's ratio and crustal seismology, *J. geophys. Res.,* **101,** 3139–3156.

Chun, K. & Yoshii, T., 1977. Crustal structure of the Tibetan Plateau; a surface-wave study by a moving window analysis, *Bull. seism. Soc. Am.,* **67,** 735–750.

Clark, M.K & Royden, L.H., 2000. Topographic ooze: building the eastern margin of Tibet by lower crustal flow, *Geology,* **28,** 703–706.

Cogan, M., Nelson, K.D., Kidd, W., Wu, C. & project INDEPTH Team, 1998. Shallow structure of the Yadong-Gulu rift, southern Tibet, from refraction analysis of INDEPTH CMP data, *Tectonics,* **17**(1), 46–61.

Coleman, M. & Hodges, K., 1995. Evidence for plateau uplift before 14 Myr ago from a new minimum age for E-W extension, *Nature,* **374,** 49–52.

Cook, F.A. & Varsek, J.I., 1994. Orogen-scale decollements, *Rev. Geophys.,* **32**, 37–60.

Cotte, N. *et al*., 1999. Determination of the crustal structure in southern Tibet by dispersion and amplitude analysis of Rayleigh waves. *Geophys. J. Int.,* **138,** 809–819.

DeCelles, P.G., Robinson, D.M., Quade, J., Ojha, T.P., Garzione, C.N., Copeland, P. & Upreti, B.N., 2001. Stratigraphy, structure, and tectonic evolution of the Himalayan fold-thrust belt in western Nepal. *Tectonics,* **20**(4), 487–509.

Edwards, M.A., Kidd, W.S.E, Li, J., Yue, Y., Wu, C. & Clark, M., 1994. Surface geology of the INDEPTH I and II seismic profiles, southern Tibet. *EOS, Trans. Am. geophys. Un.,* **75,** 632.

England, P. & Houseman, G., 1988. The mechanics of the Tibetan Plateau, *Phil. Trans. R. Soc. Lond., A,* **326,** 301–320.

England, P. & Molnar, P., 1993. Cause and effect among thrust and normal faulting, anatectic melting and exhumation in the Himalaya, in *Himalayan Tectonics*, Vol. 74, pp. 401–411, eds Treloar, P.J. & Searle, M., Geol. Soc. London Spec. Publ.

Galve, A., Sapin, M., Hirn, A., Diaz, J., Lepine, J.C., Laigle, M., Gallart, J. & Jiang, M., 2002. Complex images of Moho and variation of Vp/Vs across the Himalaya and South Tibet, from a joint receiver-function and wide-angle-reflection approach, *Geophys. Res. Lett.,* **29**(24), 2182, doi: 10.1029/2002GL015611.

Gansser, A., 1964. *Geology of the Himalayas*, Wiley Interscience, London, 289 pp.

Gao, E. *et al*., 1991. Crustal structure interpreted from the explosive seismic exploration in the Himalayas Yarlung-Zangbo area, in *Papers on Geophysics, Geology of the Himalayas*, Vol. 1, pp. 25–36, eds Li, G., Yuan, X. & Hirn, A., Geological Publishing House, Beijing, China. 298 pp.

Grujic, D., Casey, M., Davidson, C., Hollister, L.S., Kündig, R., Pavlis, T. & Schmid, S., 1996. Ductile extrusion of the Higher Himalayan Crystalline in Bhutan: evidence from quartz microfabrics, *Tectonophysics* **260**(1–3), 21–43. doi:10.1016/0040-1951(96)00074-1.

Harrison, T. M., Copeland, P., Kidd, W.S.F. & Lovera, O.M., 1995. Activation of the Nyainqentanghla shear zone: Implications for uplift of the southern Tibetan Plateau, *Tectonics,* **14,** 658–676.

Harrison, T.M., Grove, M., McKeegan, K.D., Coath, C.D., Lovera, O.M. & LeFort, P. 1999. Origin and episodic emplacement of the Manaslu intrusive complex, central Himalaya, *J. Petrol.,* **40,** 3–19.

Hauck, M.L., Nelson, K.D., Brown, L.D., Zhao, W. & Ross, A.R., 1998. Crustal structure of the Himalayan orogen at −90 degree east longitude from Project INDEPTH deep reflection profiles, *Tectonics,* **17**(4), 481–500.

Haines, S.S., Klemperer, S.L., Brown, L., Guo, J., Mechie, J., Meissner, R., Ross, A. & Zhao, W., 2003. INDEPTH III seismic data: from surface observations to deep crustal processes in Tibet. *Tectonics,* **22**(1), 1001, doi:10.1029/2001TC001305.

Hirn, A. & Sapin M., 1984. The Himalayan zone of crustal interaction: suggestions from explosion seismology, *Ann. Geophys.,* **2,** 123–130.

Hirn, A. *et al*., 1984a. Crustal structure and variability of Himalayan border of Tibet, *Nature,* **307,** 23–25.

Hirn, A., Nercessian, A., Sapin, M., Jobert, G., Xu, Z.X., Gao, E.Y., Lu, D.Y. & Teng, J.W., 1984b. Lhasa block and ordering suture: a continuation of a 500 km Moho traverse through Tibet, *Nature,* **307**(5946), 25–27.

Hirn, A., Jobert, G., Wittlinger, G., Xu, Z.X. & Gao E.Y., 1984c. Main features of the upper lithosphere in the unit between the High Himalayas and the Yarlung Zangbo Jiang suture, *Ann. Geophys.,* **2,** 113–118.

Hirn, A., Sapin, M., Jean Claude Lepine, Jordi Diaz & Jiang M., 1997. Increase in melt fraction along a south-north traverse below the Tibetan Plateau: evidence from seismology, *Tectonophysics,* **273,** 17–30.

Hodges, K.V., Parrish, R.R., Housh, T.B., Lux, D.R., Burchfiel, B.C., Royden, L.H. & Chen, Z., 1992. Simultaneous Miocene extension and shortening in the Himalayan Orogen. *Nature,* **258,** 1466–1470.

Inger, S. & Harris, N.B.W., 1993. Geochemical constraints on leucogranite magmatism in the Langtang Valley, Nepal Himalaya. *J. Petrol.,* **34,** 345–368.

Kind, R. *et al*., 1996. Evidence from earthquake data for a partially molten crustal layer in southern Tibet, *Science,* **274**(5293), 1692–1694.

Klemperer, S.L., 2006. Crustal flow in Tibet: geophysical evidence for the physical state of Tibetan lithosphere, and inferred patterns of active flow, in *Channel Flow, Ductile Extrusion and Exhumation in Continental Collision Zones*, Vol. 268, pp. 39–70, eds Law, R.D., Searle, M.P. & Godin, L., Geological Society, London, Special Publications.

Le Fort, P., 1975. Himalayas: the collided range, Present knowledge of the continental arc, *Am. J. Sci.,* **275A,** 1–44.

Lee, J. *et al*., 2000. Evolution of the Kangmar dome, southern Tibet: Structural, petrologic, and thermochronologic constraints, *Tectonics,* **19**(5), 872–895.

Lee, J., Hacker, B. & Wang, Y., 2004. Evolution of North Himalayan gneiss domes: structural and metamorphic studies in Mabja Dome, southern Tibet, *J. Struct. Geol.,* **26,** 2297–2316.

Leech, M.L., Singh, S., Jain, A.K., Klemperer, S.L., Manickavasagam, R.M., 2005. The onset of India–Asia continental collision: Early, steep subduction required by the timing of UHP metamorphism in the western Himalaya, *Earth planet. Sci. Lett.,* **234,** 83–97.

Liu, D.M., Li, D.W., Fan, X.G. & Liao, Q.A., 2009. Evolution of deformation and metamorphism during the tectono-emplacement of the granulite in the middle Himalaya orogen, *J. Jilin Univ. (Earth Sci. Edition),* **39**(4), 699–705.

Makovsky, Y. & Klemperer, S.L., 1999. Measuring the seismic properties of Tibetan bright spots: evidence for free aqueous fluids in the Tibetan middle crust, *J. geophys. Res.,* **104**(135), 10 795–10 825.

Makovsky Y., Klemperer, S.L., Huang, L.Y., Lu, D.Y. & Project Indepth Team, 1996. Structural elements of the southern Tethyan Himalaya crust from wid-angle seismic data, *Tectonics,* **15,** 997–1005.

Makovsky, Y., Klemperer, S., Ratschbacher, L. & Alsdorf, D., 1999. Mid-crust reflector on INDEPTH wide-angle profiles: an ophiolitic slab beneath the Indian-Asia suture in southern Tibet, *Tectonics,* **18**(5), 793–808.

Masek, J.G., Isacks, B.L., Fielding, E.J. & Browaeys, J., 1994. Rift flank uplift in Tibet: evidence for a viscous lower crust, *Tectonics,* **13,** 659–667.

Matthews, D. & Hirn, A., 1984. Crustal thickening in Himalayas and Caledonides, *Nature* **308**, 497–498.

Min, Z. & Wu, F.T., 1987. Nature of the upper crust beneath central Tibet, *Earth planet. Sci. Lett.,* **84**, 204–210.

Molnar, P. & Tapponnier, P., 1978. Active tectonics of Tibet, *J. geophys. Res.,* **83,** 5361–5375.

Molnar, P., England, P. & Martinod, J., 1993. Mantle dynamics, uplift of the Tibetan, and the indian monsoon, *Rev. Geophys.,* **31,** 357–396.

Monsalve, G., Sheehan, A., Schulte-Pelkum, V., Rajaure, S., Pandey, M.R. & Wu, F., 2006. Seismicity and one-dimensional velocity structure of the Himalayan collision zone: earthquakes in the crust and upper mantle. *J. geophys. Res.,* **111,** doi:10.10292005JB004062.

Nelson, K.D. & 27 co-authors, 1996. partially molten middle crust beneath southern Tibet: synthesis of project INDEPTH results, *Science,* **274,** 1684–1688.

Owens, T. J. & Zandt, G., 1997. Implications of crustal property variations for models of Tibetan plateau evolution, *Nature,* **387,** 37–43.

Pandey, M., Tandukar, R., Avouac, J., Vergne, J. & Heritier, T., 1999. Seismotectonics of the Nepal Himalaya from a local seismic network, *J. Asian Earth Sci.,* **17,** 703–712.

Patiño Douce, A.E. & Harris, N., 1998. Experimental constraints on Himalayan anatexis, *J. Petrol.,* **39,** 689–710.

© 2010 The Authors, *GJI*, **181,** 1247–1260
Journal compilation © 2010 RAS

Ratschbacher, L., Frisch, W., Liu, G. & Chen, C., 1994. Distributed deformation in southern and western Tibet during and after India-Asia collision, *J. geophys. Res.,* **99,** 19817–19945.

Rodgers, A.J. & Schwartz, S.Y., 1997. Low crustal velocities and mantle lithospheric variations in southern Tibet from regional Pnl waveforms, *Geophys. Res. Lett.,* **24,** 9–12.

Sapin, M. & Hirn, A., 1997. Seismic structure and evidence for eclogitization during the Himalayan convergence, *Tectonophysics,* **273,** 1–16.

Sapin, M., Wang, X., Hirn, A. & Xu, Z., 1985. A seismic sounding in the crust of the Lhasa block, Tibet, *Ann. Geophys.,* **3**(5), 637–646.

Schulte-Pelkum, V., Monsalve, G., Sheehan, A., Pandey, M.R., Sapkota, S., Bilham, R. & Wu, F., 2005. Imaging the Indian subcontinent beneath the Himalaya, *Nature,* **435,** 1222–12225.

Searle, M., Corfield, R.I., Stephenson, B. & McCarron, J., 1997. Structure of the north Indian continental margin in the Ladakh–Zanskar Himalayas: implications for the timing of obduction of the Spontang ophiolite, India–Asia collision and deformational events in the Himlaya, *Geol. Mag.,* **134,** 297–316.

Searle, M.P., 1983. Stratigraphy, structure and evolution of the Tibetan–Tethys zone in Zanskar and the Indus suture zone in the Ladakh Himalaya, *Trans. Roy. Soc. Edinburgh,* **73,** 205–219.

Searle, M.P., Cooper, D.J.W. & Rex, A.J., 1988. Collision tectonics of the Ladakh Zanskar Himalaya. *Phil. Trans. Roy. Soc. Lond., Ser. A,* **326,** 117–150.

Searle, M.P. *et al*., 1987. The closing of Tethys and the tectonics of the Himalaya, *Geol. Soc. Am. Bull.,* **98,** 678–701.

Srivastava, P. & Mitra, G., 1994. Thrust geometries and deep structure of the outer and lesser Himalaya, Kumaon and Garhwal (India): implications for evolution of the Himalayan fold-and-thrust belt, *Tectonics* **13**(1), 89–109.

Tapponnier, P. & Molnar, P., 1977. Active faulting and tectonics in China, *J. geophys. Res.,* **82,** 2905–2930.

Tapponnier, P., Peltzer, G., Le Dayn, A.Y., Armijo, R. & Cobbold, P., 1982. Propagating extension tectonics in Asia: new insights from simple experiments with plasticine, *Geology,* **110,** 611–616.

Teng, J.W., Xiong, S.B. & Yin Z.X., 1985. Seismic velocity distribution and crustal velocity in Xizang (Tibet) Plateau, *Chin. J. Geophys.*, **28**(1), 16–27 (in Chinese and with English abstract).

Teyssier, C. & Whitney, D.L., 2002. Gneiss domes and orogeny, *Geology,* **30,** 1139–1142.

Thiede, R.C., Ramón Arrowsmith, J., Bodo Bookhagen, Michael McWilliams, Edward, R., Sobel, Manfred, R. & Strecker, 2006. Dome formation and extension in the Tethyan Himalaya, Leo Pargil, northwest India, *GSA Bull.,* **118**(5/6), 635–650; doi:10.1130/B25872.

Unsworth, M.J., Jones, A.G., Wei, W., Marquis, G., Gokarn, S.G., Spratt, J.E. & the INDEPTH-MT team, 2005. Crustal rheology of the Himalaya and southern Tibet inferred from magnetotelluric data, *Nature,* **438,** doi:10.1038/nature04154.

Wang, C.Y., Flesch, L.M., Silver, P.G., Chang, L.J. & Chan, W.W., 2008. Evidence for mechanically coupled lithosphere in central Asia and resulting implications, *Geology,* **36,** 363–366.

Wu, C., Nelson, K.D., Wortman, G., Samson, S.D., Yue, Y.J., Li, J.X., Kidd, W.S.F. & Edwards, M.A., 1998. Yadong cross structure and South Tibetan Detachment in the east central Himalaya (89–90 degree E), *Tectonics,* **17**(1), 28–45.

Xiong, S., Teng, J. & Yin, Z., 1985. The thickness of the crust and undulation of discontinuity in Xizang (Tibet) plateau, *Chin. J. Geophys.*, **28**(1), 16–27 (in Chinese and with English abstract).

Yin, A., 2000. Mode of Cenozoic east-west extension in Tibet suggesting a common origin of rifts in Asia during the Indo-Asia collision, *J. geophys. Res.,* **105**(B9), 21 745–21 759.

Yin, A. & Harrison, T.M., 2000. Geologic evolution of the HimalayanTibetan orogen, *Annu. Rev. Earth planet. Sci.,* **28,** 211–280.

Yuan, X., Ni, J., Kind, R., Mechie, J. & Sandvol, E., 1997. Lithospheric and upper mantle structure of southern Tibet from a seismological passive source experiment, *J. geophys. Res.,* **102**(B12), 27 491–27 500.

Zhang, H., Harris, N., Parrish, R., Kelley, S., Zhang, L., Rogers, N., Argles, T. & King, J., 2004. Causes and consequences of protracted melting of the mid-crust exposed in the North Himalayan antiform, *Earth planet. Sci. Lett.,* **228,** 195–212.

Zhang, Z. & Klemperer, S., 2005. West–east variation in crustal thickness in northern Lhasa block, central Tibet, from deep seismic sounding data, *J. geophys. Res.,* **110**(B9), B09403, doi:10.129/2004JB003139.

Zhang, Z., Wang, Y., Chen, Y., Houseman, G., Tian, X., Wang, E. & Teng, J., 2009. Crustal structure across Longmenshan fault belt from passive source seismic profiling, *Geophys. Res. Lett.,* **36,** L17310, doi:10.1029/2009GL039580.

Zhang, Z., Yuan, X., Chen, Y., Tian, X., Kind, R., Li, X. & Teng, J., 2010. Seismic signature of the collision between the east Tibetan escape flow and the Sichuan Basin, *Earth planet. Sci. Lett.*, **292,** 254–264, doi:10.1016/j.epsl.2010.01.046.

Zhao, L., Sen, M.K., Stoffa, P. & Frohlich, C., 1996. Application of very fast simulated annealing to the determination of the crustal structure beneath Tibet, *Geophys. J. Int.,* **125,** 355–370.

Zhao, W.J., INDEPTH group, 2001. *Deep Structure and Formation Study under Himalaya Mountain and Indus-Yarluzanbo Suture Belt*, Geological Publisher (in Chinese), 369 pp.

Zhao, W.J., Nelson, K.D. & Project INDEPTH Team, 1993. Deep seismic reflection evidence for continental underthrusting beneath southern Tibet, *Nature,* **366,** 557–559.

Zhao, W.L. & Morgan, W.J., 1987. Injection of India crust into Tibetan lower crust, *Tectonics,* **6,** 489–504.

© 2010 The Authors, *GJI*, **181,** 1247–1260
Journal compilation © 2010 RAS